PLANET ENGULFMENT BY ∼1.5–3 $M_\odot$ RED GIANTS

M. KUNITOMO[1], M. IKOMA[1], B. SATO[1,2], Y. KATSUTA[3], AND S. IDA[1]

[1] Department of Earth and Planetary Sciences, Tokyo Institute of Technology (TokyoTech), 2-12-1 Ookayama,
Meguro-ku, Tokyo 152-8551, Japan; mikoma@geo.titech.ac.jp
[2] Global Edge Institute, Tokyo Institute of Technology (Tokyo Tech), 2-12-1 Ookayama,
Meguro-ku, Tokyo 152-8551, Japan
[3] Department of Cosmosciences, Hokkaido University, Kita 10 Nishi 8, Kita-ku,
Sapporo 060-0810, Japan
Received 2010 December 16; accepted 2011 June 1; published 2011 August 4

ABSTRACT

Recent radial-velocity surveys for GK clump giants have revealed that planets also exist around ∼1.5–3 $M_\odot$ stars. However, no planets have been found inside 0.6 AU around clump giants, in contrast to solar-type main-sequence stars, many of which harbor short-period planets such as hot Jupiters. In this study, we examine the possibility that planets were engulfed by host stars evolving on the red-giant branch (RGB). We integrate the orbital evolution of planets in the RGB and helium-burning phases of host stars, including the effects of stellar tide and stellar mass loss. Then we derive the critical semimajor axis (or the survival limit) inside which planets are eventually engulfed by their host stars after tidal decay of their orbits. Specifically, we investigate the impact of stellar mass and other stellar parameters on the survival limit in more detail than previous studies. In addition, we make detailed comparisons with measured semimajor axes of planets detected so far, which no previous study has done. We find that the critical semimajor axis is quite sensitive to stellar mass in the range between 1.7 and 2.1 $M_\odot$, which suggests a need for careful comparison between theoretical and observational limits of the existence of planets. Our comparison demonstrates that all planets orbiting GK clump giants that have been detected are beyond the survival limit, which is consistent with the planet-engulfment hypothesis. However, on the high-mass side ($>2.1M_\odot$), the detected planets are orbiting significantly far from the survival limit, which suggests that engulfment by host stars may not be the main reason for the observed lack of short-period giant planets. To confirm our conclusion, the detection of more planets around clump giants, especially with masses $\gtrsim 2.5M_\odot$, is required.

Key words: planets and satellites: formation – stars: evolution

Online-only material: color figures

1. INTRODUCTION

Detection of a significant number of exoplanets orbiting Sun-like stars (FGK dwarfs) has helped us to improve our understanding of the origins and diversity of planetary systems. Statistics on detected planets suggest the presence of several different populations and correlations. This has motivated theorists to synthesize planet populations by integrating the formation process from planetesimals to planets (Ida & Lin 2004a, 2004b, 2005, 2008a, 2008b, 2010; Kennedy & Kenyon 2008a, 2008b; Mordasini et al. 2009a, 2009b). Comparison with statistical properties from observations has then enabled us to calibrate theories for planet formation.

As for heavier stars such as BA dwarfs, the situation is somewhat different. Precise radial-velocity measurements of heavier stars are not successful because of the lack of absorption lines on their hot photospheric surfaces. Instead, efforts have been made to find planets around GK giants that used to be BA dwarfs on the main sequence (MS). Thus, comparisons between observations and theories of heavier stars are not straightforward, unlike in the case of FGK dwarfs. This means we have to take into account modifications to orbital configurations of planets during their host stars' evolution.

According to recent radial-velocity surveys for GK clump giants, it appears that there is a lack of giant planets inside 0.6 AU (Sato et al. 2010 and references therein). Such a deficit is not seen around Sun-like stars which often harbor short-period planets such as hot Jupiters. It is unclear whether the deficit is primordial—namely, short-period giant planets (SPGPs) are not formed around BA dwarfs originally; otherwise, short-period planets are removed during host stars' evolution. The latter possibility is the focus of this paper.

A star evolves off the MS toward the red-giant branch (RGB) after the exhaustion of hydrogen at its center. Then, once the helium ignites, the star enters the next central nuclear burning phase, which is sometimes called the helium-burning (HeB) phase. Most of the clump giants with detected planets are thought to be in the HeB. Before reaching the HeB, namely, in the RGB phase, the star expands substantially, becomes highly luminous, and may lose substantial mass, which should affect orbits of surrounding planets.

The evolution and fate of planets orbiting stars in the RGB phase have been investigated in the context of the survival of the Earth. Based on his simple estimation, Vila (1984), followed by a somewhat detailed argument from Goldstein (1987), showed that the Earth would lose its momentum quickly in the extending envelope of the Sun before the envelope starts to shrink again. This means the Earth would be unable to escape from the Sun once engulfed. These studies suggested the need for a detailed simulation of the Sun's evolution. The Sun's evolution, including solar mass loss, was simulated in detail by Sackmann et al. (1993), who demonstrated that the decrease in the solar mass is effective in pushing the terrestrial planets other than Mercury outward and preventing them from being

engulfed by the expanding Sun. Later, building on theories for the formation of close binaries (e.g., Livio 1982; Livio & Soker 1983, 1984), Rasio et al. (1996) incorporated the tide raised on the Sun and then demonstrated that Venus is likely to fall into the Sun because of the solar tide enhanced by the expansion of the envelope, while Earth's fate remained inconclusive, depending on unconstrained parameters for tide. Other effects such as the gravitational drag, ram pressure, wind accretion (Vila 1984; Duncan & Lissauer 1998), and orbital instability due to secular perturbation (Duncan & Lissauer 1998) are known to be negligible. Note that the last effect could be important in extrasolar planetary systems, depending on orbital configurations.

To understand the observed lack of SPGPs around GK clump giants, Sato et al. (2008a) and Villaver & Livio (2009) investigated the orbital evolution of planets around intermediate-mass RGB stars in a similar manner to Rasio et al. (1996). They demonstrated that SPGPs underwent orbital decay due to stellar tide, ending up being swallowed by their host stars. In particular, Villaver & Livio (2009) derived a critical semimajor axis, a_{crit} (note that they called it a minimum semimajor axis denoted by a_{min}), beyond which planets evade engulfment by their host stars during the RGB phase: in four cases of different stellar initial masses, $M_{\star,i}$ (i.e., 1, 2, 3, and 5 $M_\odot$), the values of a_{crit} that they derived for Jovian-mass planets were 3.0, 2.1, 0.18, and 0.45 AU, respectively. Then, without a detailed comparison of a_{crit} with the orbital distribution of known planets around GK clump giants, they concluded that engulfment by host stars may be responsible for the observed lack of SPGPs inside 0.6 AU and any ad hoc mechanism for not forming SPGPs may not be required.

In this paper, to verify the planet-engulfment hypothesis, we make a detailed comparison of the theoretical limit of survival (namely, a_{crit}) with semimajor axes of the planets detected so far around GK clump giants. The masses of these giants range from ~1.5 to 3 $M_\odot$. As known in the study of stellar evolution (e.g., Kippenhahn & Weigert 1990), the RGB-tip radius is sensitive to stellar mass in such a range. Given that stellar tide depends strongly on the stellar radius (see Section 2), the limit of survival from engulfment by host stars should be sensitive to host stars' masses, which implies the need for a detailed comparison between the theoretical and observational limits. It should be noted that Nordhaus et al. (2010) recently made a thorough study of the tidal evolution of the orbits of planets around post-MS stars. Their focus, however, was on planets around white dwarfs that survive engulfment by asymptotic giant branch (AGB) stars. Planets around RGB or HeB stars that have not yet entered the AGB phase are of interest in this paper.

This paper is organized as follows. In Section 2, we first describe our physical model and computation method for simulating the orbital evolution of a planet around its host star that is evolving off the MS. In Section 3, we derive a critical semimajor axis beyond which planets survive the host stars' RGB/HeB phase, and investigate its sensitivity to stellar mass and other parameters. In Section 4, we compare the derived survival limit with measured semimajor axes of the detected planets. The comparison suggests that planet engulfment may not be the main reason for the observed paucity of SPGPs, apart from statistical sufficiency. In Section 5, we evaluate the impacts of several uncertainties on the survival limit and find that our conclusion is not affected by them. In Section 6, we mention the possibility of a stellar-mass-dependent formation process

that may account for the observed paucity of SPGPs. Finally, in Section 7, we summarize this paper, claiming the need for more planet samples around giants of >2.5 $M_\odot$ to confirm the validity of our findings.

2. PHYSICAL MODEL AND COMPUTATION METHOD

We simulate the evolution of the orbits of planets during their host stars' evolution. We assume circular orbits, because our focus is on the semimajor axis in this study. The eccentricities of planets detected around the GK clump giants that we target in this study are as small as 0.25. Such a small eccentricity has a small effect on the evolution of the semimajor axis. The impact of the finite eccentricity on the limit of survival is evaluated in Section 5.3. Note that previous studies (Villaver & Livio 2009; Nordhaus et al. 2010) also assumed zero eccentricities.

We consider the effects of stellar tide and mass loss on the planetary orbit. We neglect other competing processes such as the frictional and gravitational drag forces by stellar wind and change in the planet mass due to stellar-wind accretion and evaporation, which were evaluated to be negligible by Villaver & Livio (2009) and Duncan & Lissauer (1998). Thus, we integrate the equation

$$\frac{1}{a}\frac{da}{dt} = -6\frac{k}{T}\frac{M_p}{M_\star}\left(1 + \frac{M_p}{M_\star}\right)\left(\frac{R_\star}{a}\right)^8 - \frac{\dot{M}_\star}{M_\star} \quad (1)$$

from the zero-age MS of the host star of a given mass. In the above equation, a is the semimajor axis, t is time, M_p is the planet's mass, $M_\star$ and $R_\star$ are the mass and radius of the host star, respectively, k is the apsidal motion constant, and T is the eddy turnover timescale (see below). The first term on the right-hand side represents the effect of stellar tide (Hut 1981). Since RGB stars are slow rotators, we assume no stellar rotation, which means that the stellar tide always causes orbital decay of the planet.

As for the parameters for stellar tide such as k and T, following Rasio et al. (1996) and Villaver & Livio (2009), we adopt the turbulent viscosity,

$$k = \frac{f}{6}\frac{M_{env}}{M_\star}, \quad (2)$$

where M_{env} is the mass in the convective envelope and f is given by

$$f = \min\left[1, \left(\frac{P}{2T}\right)^2\right] \quad (3)$$

with P being the orbital period. The eddy turnover timescale T is given by

$$T = \left[\frac{M_{env}(R_\star - R_{env})^2}{3L_\star}\right]^{1/3}, \quad (4)$$

where R_{env} is the radius at the base of the convective zone and $L_\star$ is the stellar intrinsic luminosity. The factor f is introduced to weaken the stellar tide when the orbital period is shorter than the eddy turnover timescale. However, how to deal with such fast tides is a matter of debate (e.g., Zahn 2008). We discuss the impact of the uncertainties of f on the survival limit in Section 5.1.

The second term on the right-hand side of Equation (1) represents orbital migration due to stellar mass loss ($\dot{M}_\star < 0$). We use the Reimers' parameterization for stellar mass loss
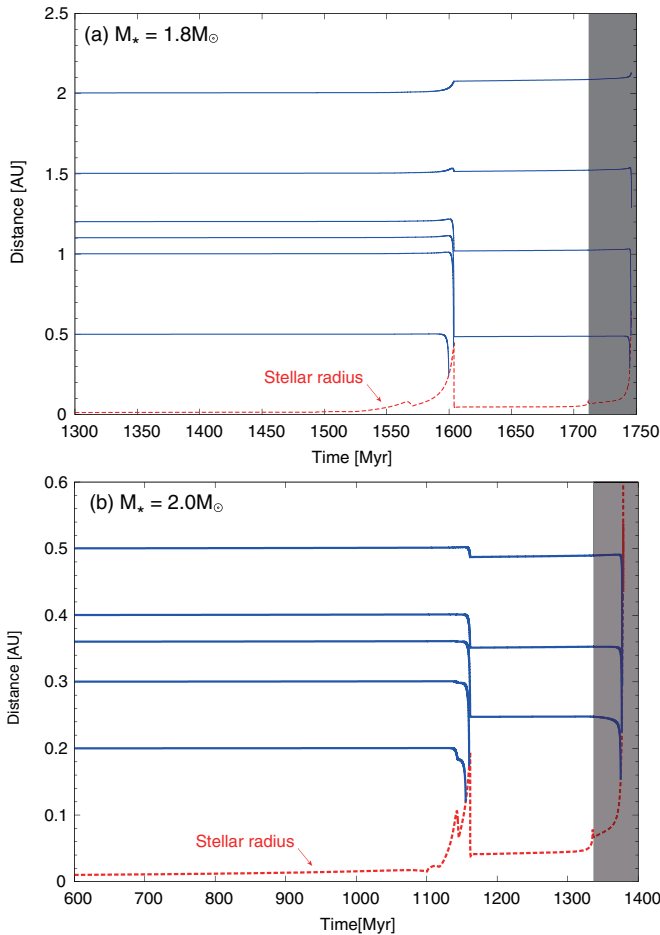
Figure 1. Orbital evolution of 1 M_J planets with different initial semimajor axes (solid lines) for $M_\star = $ (a) 1.8 $M_\odot$ and (b) 2.0 $M_\odot$; the metallicity, $Z_\star$, is 0.02 in both cases. Dashed lines represent the evolution of stellar radii.

(A color version of this figure is available in the online journal.)

(Reimers [1975]), namely,

$$\dot{M}_\star = -4 \times 10^{-13} \eta \left(\frac{L_\star}{L_\odot} \right) \left(\frac{R_\star}{R_\odot} \right) \left(\frac{M_\star}{M_\odot} \right)^{-1} M_\odot \, \mathrm{yr}^{-1}, \quad (5)$$

where η is the mass-loss parameter of order unity.

In this study, we simulate stellar evolution directly with the code MESA version 2258 (Paxton et al. [2011]) to calculate $M_\star(t)$, $R_\star(t)$, $L_\star(t)$, $\dot{M}_\star(t)$, $M_{\mathrm{env}}(t)$, and $R_{\mathrm{env}}(t)$. We adopt the mass-loss parameter $\eta = 0.6$ and the mixing-length parameter $\alpha = 1.5$. We include the effects of convective overshooting, following MESA's prescription where the overshoot parameters are set to be 0.0128 at the bottom of non-burn regions and 0.014 at all the other boundaries. Several different stellar-evolution models that are simulated with different numerical codes are available in the literature and online. Villaver & Livio ([2009]) used a stellar-evolution code other than MESA. We discuss the differences between the codes and their impacts on the survival limit in Section 5.2.

3. THEORETICAL LIMIT OF SURVIVAL

3.1. Orbital Evolution

We derive the theoretical limit of survival from engulfment by evolving host stars. Figure 1 shows examples of the orbital evolution of planets around stars with initial masses, $M_{\star,i}$, of

(a) 1.8 $M_\odot$ and (b) 2.0 $M_\odot$; the metallicity is 0.02. We have integrated the orbit of a 1 M_J planet (M_J: Jupiter's mass) with different initial semimajor axes (solid lines) from the host-star zero-age MS until the planet's semimajor axis falls below the stellar radius ($a < R_\star$) or until the AGB thermal pulse occurs. The evolution of the stellar radii is represented by the dashed lines.

Although we have continued the simulations after the end of the HeB phase (gray areas in the figure), our interest in this study is whether planets survive the RGB and HeB phases of their host stars. This is because the planet-harboring GK clump giants that we target for the comparison of our survival limit with the semimajor axes of their planets are thought to be in the HeB or RGB phases, as stated in Section 1. As for the orbital evolution of planets around AGB stars, Nordhaus et al. ([2010]) made a thorough investigation of this.

As seen in Figure 1(a), the 1.8 $M_\odot$ star expands up to 0.5 AU at the RGB tip. As the stellar radius becomes large, tidal decay is rapidly enhanced (Equation (1)), so that the star consequently swallows planets whose initial semimajor axes, a_i, are smaller than 1.1 AU. The planet that starts out at 1.1 AU is tidally pulled by the host star, but it barely survives the RGB tip and remains in the HeB phases. Outer planets (e.g., $a_i = 2.0$ AU) are found to be pushed outward because of stellar mass loss; the effect is, however, small, unlike in the case of 1 $M_\odot$ stars, as also noted previously (Sato et al. [2008a]; Villaver & Livio [2009]; Nordhaus et al. [2010]). As for 2 $M_\odot$ stars, the RGB-tip radius is as small as 0.20 AU (Figure 1(b)). As a consequence, even a planet starting out at 0.36 AU can avoid engulfment during the RGB/HeB phases of these stars.
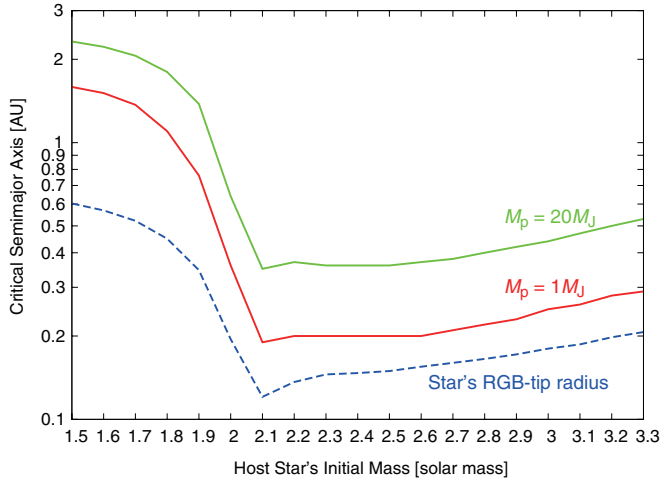
We define a critical initial semimajor axis (a_{crit}) below which planets end up being engulfed by their host stars at some point in the RGB or HeB phases. For the above two examples, $a_{\mathrm{crit}} = 1.1$ AU around the 1.8 $M_\odot$ star, while $a_{\mathrm{crit}} = 0.36$ AU around the 2 $M_\odot$ star. It is thus illustrated that the survival limit is rather sensitive to the host star's mass. Furthermore, comparing Figure 1(b) with the upper right panel of Figure 1 of Villaver & Livio ([2009]), one notices that the value of a_{crit} derived here for the 2 $M_\odot$ star is considerably different from that derived by Villaver & Livio ([2009]), who estimated a_{crit} to be 2.1 AU instead of 0.36 AU. The reason for this difference is discussed in Section 5.2.

For comparison with semimajor axes of a detected planets, the above definition of a_{crit} may be inappropriate because it is the initial value of the semimajor axis of a planet that barely survives the host-star's RGB tip. As shown in the above figure, a planet's semimajor axis after the RGB tip is lower than its initial value. However, the probability that such planets are detected should be low. Because of the unambiguity of the definition, we decide to use the critical semimajor axis defined above.

3.2. Critical Semimajor Axes

Figure 2 shows the relation between a_{crit} and $M_{\star,i}$ for $M_p = 1 M_J$ and 20 M_J. The stellar RGB-tip radius (R_{tip}) is also shown by the dashed line.

First, one notices that the curves for a_{crit} are similar in shape to that for R_{tip}. This is because the tidal decay rate of the planetary orbit is quite sensitive to the stellar radius (see Equation (1)). This means that in most cases, planet engulfment occurs right around the RGB tip of the host star, at which the stellar radius reaches a maximum during the RGB/HeB phases. To see this more clearly, we derive an approximate expression of a_{crit} as follows. From Equation (1), a typical decay timescale (τ_{decay})

Figure 2. Critical initial semimajor axis, $a_{\rm crit}$, inside which planets are engulfed by host stars before reaching the end of the HeB phase for two choices of planetary mass, M_p, namely, $M_p = 1\,M_{\rm J}$ and $20\,M_{\rm J}$. For comparison, the RGB-tip radius of the host star is shown by the dashed line. The stellar metallicity is 0.02 in the calculations.

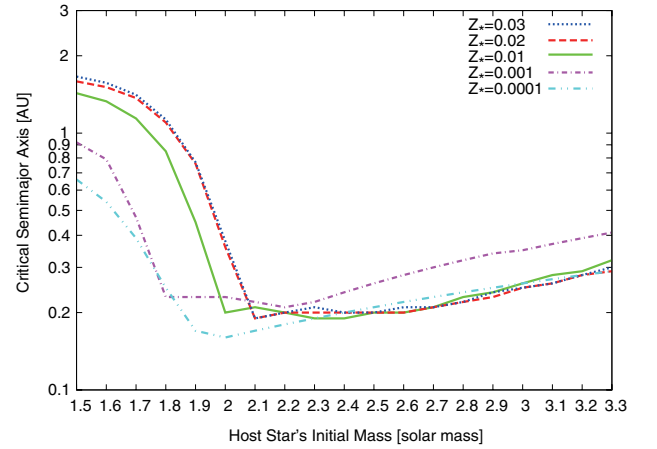(A color version of this figure is available in the online journal.)

can be expressed by

$$\tau_{\rm decay} \sim \frac{T}{6k}\frac{M_\star}{M_p}\left(\frac{R_\star}{a}\right)^{-8}, \tag{6}$$

provided the mass-loss effect is negligible. If $\tau_{\rm decay}$ is comparable to the typical duration of the RGB phase ($\tau_{\rm RGB}$), then the planet is engulfed by its host star. Thus, $a_{\rm crit}$ would be expressed as

$$a_{\rm crit} = \left(\frac{12\pi^3\sigma}{G}\right)^{1/5}\frac{T_{\rm eff}^{4/5}M_p^{1/5}}{M_\star^{3/5}}\tau_{\rm RGB}^{1/5}R_{\rm tip}^{8/5}$$

$$= 0.11\left(\frac{R_{\rm tip}}{0.1\,{\rm AU}}\right)^{8/5}\left(\frac{M_\star}{2\,M_\odot}\right)^{-3/5}\left(\frac{\tau_{\rm RGB}}{5\,{\rm Myr}}\right)^{1/5}$$

$$\times\left(\frac{M_p}{M_{\rm J}}\right)^{1/5}\left(\frac{T_{\rm eff}}{4000\,{\rm K}}\right)^{4/5}\,{\rm AU}. \tag{7}$$

In deriving this equation, based on our numerical results, we have assumed that $M_{\rm env} \sim M_\star$ and $R_{\rm env} \sim 0$ in Equations (2) and (4) and used $T \sim (M_\star R_{\rm tip}^2/3L_{\rm tip})^{1/3}$ with the stellar RGB-tip luminosity $L_{\rm tip} = 4\pi\sigma R_{\rm tip}^2 T_{\rm eff,tip}^4$ and $k \sim f/6 = (P/2T)^2/6$ (see Equations (2)–(4)). Equation (7) confirms that $R_{\rm tip}$ is the most important factor and that the others have a minor impact on $a_{\rm crit}$. Note that we have found that $\tau_{\rm RGB}$ is not sensitive to stellar mass; for example, the periods during which $R_\star(t) > 0.5\,R_{\rm tip}$ in the RGB phase are 4.3 Myr, 9.7 Myr, and 5.2 Myr for 1.5 $M_\odot$, 2.0 $M_\odot$, and 3.0 $M_\odot$ stars with $Z_\star = 0.02$, respectively. It is worth noting that Equation (7) agrees well with the numerical values of $a_{\rm crit}$ on the high-mass side in Figure 2; the differences are less than 10% for $M_\star \gtrsim 2.0\,M_\odot$. On the low-mass side (i.e., $M_\star < 2.0M_\odot$), the differences are bigger; for example, Equation (7) predicts that $a_{\rm crit}$ is bigger by about 25% (0.4 AU) than its numerical value for $M_\star = 1.5\,M_\odot$. This is because the stellar mass loss is relatively effective in pushing planets outward in the low-mass cases.

Next, as seen in Figure 2, there is a sharp transition in between 1.7 $M_\odot$ and 2.1 $M_\odot$: $a_{\rm crit}$ changes by approximately one order of magnitude in such a narrow mass range. The transition

Figure 3. Critical initial semimajor axis, $a_{\rm crit}$, inside which planets are engulfed by host stars before reaching the end of the HeB phase for five choices of stellar metallicity, $Z_\star$. Dotted, dashed, solid, dot-dashed, and double-dot-dashed lines represent the results for $Z_\star = 0.03$, 0.02, 0.01, 0.001, and 0.0001, respectively. In these calculations, the planet's mass is 1 $M_{\rm J}$.

(A color version of this figure is available in the online journal.)
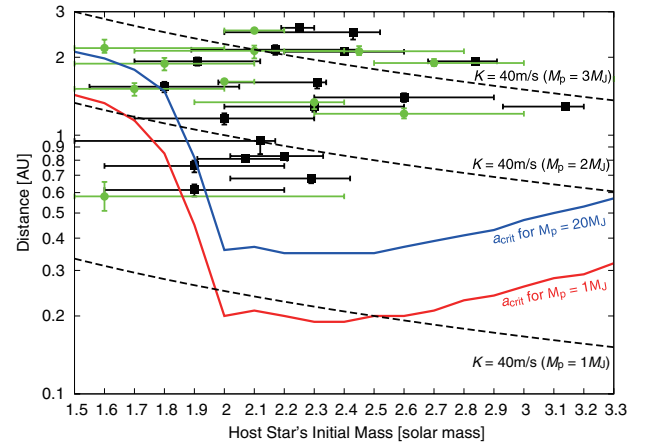
Figure 4. Comparison between the theoretical survival limits and the semimajor axes of known planets around clump giants. The solid lines represent the critical initial semimajor axes, $a_{\rm crit}$, for stellar metallicity $Z_\star = 0.01$ and planetary mass $M_p = 1$ and $20\,M_{\rm J}$. The semimajor axes of the planets are represented by symbols with error bars: filled squares and circles correspond to values from the literature and those re-evaluated with MESA, respectively. The dashed lines represent a radial-velocity semi-amplitude of 40 m s^{-1} for $M_p = 1$, 2, and 3 $M_{\rm J}$.

(A color version of this figure is available in the online journal.)

corresponds to that of $R_{\rm tip}$ which is related to the thermal state of the stellar helium core. A low-mass star of $\lesssim 2\,M_\odot$ has a degenerate helium core after exhausting its central hydrogen and undergoes helium flash, which causes significant expansion in its RGB phase; in contrast, an intermediate-mass star of $\gtrsim 2\,M_\odot$ soon starts burning 3α at its center instead of undergoing helium flash, so for these stars $R_{\rm tip}$ is relatively small.

Finally, the dependence of $a_{\rm crit}$ on $M_{\star,i}$ is qualitatively the same regardless of stellar metallicity ($Z_\star$), but $a_{\rm crit}$ decreases with decreasing $Z_\star$, as illustrated in Figure 3. This is also related to the dependence of $R_{\rm tip}$ on $Z_\star$. Because of the low opacity in the atmosphere and the low efficiency of the CNO cycle in the hydrogen-burning shell, metal-poor RGB stars expand less compared to metal-rich RGB stars.

4. COMPARISON WITH OBSERVATIONS

In Figure 4 the critical semimajor axis, $a_{\rm crit}$, which we have calculated numerically, is compared with the measured

semimajor axes of planets that have been detected around GK clump giants: $a_{\rm crit}$ for $M_p = 1\,M_J$ and $20\,M_J$ and $Z_\star = 0.01$ are represented by solid lines. The measured semimajor axes are represented by symbols with error bars—filled squares are data from the literature, while filled circles are values that we have re-evaluated using theoretical evolution curves generated with MESA. Published values of the stellar masses were evaluated based on other stellar codes (Girardi et al. 2000; Lejeune & Schaerer 2001).

Re-evaluation of stellar masses has been performed for self-consistency; this means that our values are never more reasonable than the published ones. Because stars of interest in this study are located in a region crowded with evolutionary curves in the H-R diagram, it is natural that the estimation of stellar mass includes a large uncertainty, which is beyond the scope of this study. Note that the three different codes, namely, MESA, Girardi et al.'s (2000), and Lejeune & Schaerer's (2001) yield similar values of $a_{\rm crit}$, as found in Section 5.2. The evaluated values of stellar masses are listed in Table 1. As a result of stellar-mass re-evaluation, planetary masses and semimajor axes are also changed. These values are also listed in Table 1. In comparing observational data with theoretical curves, we have assumed that stars are located in the HeB phase or post-HeB phases.

Figure 4 indicates two important things. First, one finds that almost all the symbols are above the curves of $a_{\rm crit}$. Although the mean values for a few planets are smaller than $a_{\rm crit}$, those error bars extend out to the curves of $a_{\rm crit}$. Second, one realizes that on the high-mass side (i.e., $M_\star > 2.1\,M_\odot$), planets exist far above $a_{\rm crit}$. There seems to be a gap between the theoretical survival limit and the observed existence limit of planets. Thus, our comparison with observations suggests that planet engulfment by host stars may not be the main reason for the lack of SPGPs, at least for $M_\star > 2.1\,M_\odot$. Note that we have to keep in mind that the number of planets may still be statistically insufficient.

The presence of the gap is not due to observational biases. Clump giants typically show an intrinsic radial-velocity variability of $\sigma = 10$–$20\ {\rm m\,s^{-1}}$ (Sato et al. 2005). Given that we can only detect planets that impart a radial-velocity semi-amplitude of $K > 40\ {\rm m\,s^{-1}}$ (i.e., 2σ) to their host stars, we indicate the detection limits by dashed lines for $M_p = 1, 2,$ and $3\,M_J$ in the figure. While the detectable limit for planets of $\leqslant 1\,M_J$ is below $a_{\rm crit}$, that for planets of $\geqslant 2\,M_J$ is significantly above $a_{\rm crit}$. Because the masses of the planets shown in the figure are all more than $2\,M_J$, the gap that we have found is not due to such observational biases.

5. SENSITIVITY TO UNCERTAINTIES

5.1. Tidal Dissipation

For tidal dissipation, this study is based on the widespread idea of turbulent viscosity (Equations (2)–(4)). It remains uncertain how to deal with fast tide when the planetary orbital period, P, is shorter than the eddy turnover timescale, T. For such a situation to be taken into account, the factor f is added in Equation (1) to weaken the stellar tide. We have adopted Kolmogorov scaling, namely, $f \propto (P/T)^2$, which supposes that only small eddies whose intrinsic turnover times are shorter than the orbital period contribute to the tidal dissipation (Goldreich & Nicholson 1977). However, the Kolmogorov picture is known to be too simplified for the turbulent viscosity. The dependence of the viscosity on P/T is a matter of debate (e.g., Zahn 2008; Penev et al. 2007 and references therein). For example, recent

Table 1
Properties of Stars and Planets Re-evaluated

Stellar Name	$M_\star{}^a$ $(M_\odot)$	$M_\star$ $(M_\odot)$	$M_p \sin i$ (M_J)	a (AU)	Ref.[b]
11 Com[c]	$3.14^{+0.06}_{-0.21}$	$2.6^{+0.4}_{-0.3}$	$17.1^{+1.7}_{-1.3}$	$1.21^{+0.06}_{-0.05}$	(1),(2)
11 UMi[d]	$1.8^{+0.25}_{-0.25}$	$1.7^{+0.3}_{-0.3}$	$10.8^{+1.2}_{-1.3}$	$1.51^{+0.09}_{-0.09}$	(3)
14 And[c]	$2.20^{+0.13}_{-0.18}$	$1.2^{+0.2}_{-0.3}$	$3.20^{+0.4}_{-0.6}$	$0.68^{+0.03}_{-0.06}$	(4),(2)
18 Del[c]	$2.25^{+0.06}_{-0.05}$	$2.1^{+0.1}_{-0.1}$	$9.84^{+0.3}_{-0.3}$	$2.54^{+0.04}_{-0.04}$	(5),(2)
81 Cet[c]	$2.43^{+0.09}_{-0.43}$	$1.6^{+0.4}_{-0.2}$	$4.01^{+0.6}_{-0.3}$	$2.17^{+0.17}_{-0.09}$	(4),(2)
HD 102272[d]	$1.9^{+0.3}_{-0.3}$	$1.6^{+0.3}_{-0.3}$	$5.26^{+1.6}_{-1.2}$	$0.58^{+0.08}_{-0.07}$	(6)
HD 104985[c]	$2.12^{+0.05}_{-0.63}$	NA			(5),(2)
HD 110014[d]	$2.17^{+0.28}_{-0.28}$	$2.1^{+0.3}_{-0.4}$	$10.9^{+1.0}_{-1.4}$	$2.12^{+0.09}_{-0.15}$	(7)
HD 119445[e]	$3.9^{+0.4}_{-0.4}$	$3.5^{+0.3}_{-0.2}$	$35.0^{+2.0}_{-1.4}$	$1.65^{+0.05}_{-0.03}$	(8)
HD 11977[d]	$1.91^{+0.21}_{-0.21}$	$1.8^{+0.3}_{-0.3}$	$6.29^{+0.7}_{-0.7}$	$1.89^{+0.10}_{-0.11}$	(9)
HD 145457[e]	$1.9^{+0.3}_{-0.3}$	$1.0^{+0.4}_{-0.1}$	$1.89^{+0.5}_{-0.1}$	$0.61^{+0.08}_{-0.02}$	(10)
HD 17092[d]	$2.3^{+0.3}_{-0.3}$	$1.55^{+0.65}_{-0.25}$	$3.53^{+0.9}_{-0.4}$	$1.13^{+0.14}_{-0.06}$	(11)
HD 173416[e]	$2.0^{+0.3}_{-0.3}$	$1.3^{+0.4}_{-0.4}$	$2.03^{+0.4}_{-0.4}$	$1.00^{+0.10}_{-0.11}$	(12)
HD 180314[e]	$2.6^{+0.3}_{-0.3}$	$2.3^{+0.1}_{-0.4}$	$20.3^{+0.6}_{-2.4}$	$1.34^{+0.02}_{-0.08}$	(10)
HD 62509[c]	$2.31^{+0.03}_{-0.33}$	$2.0^{+0.1}_{-0.2}$	$2.63^{+0.1}_{-0.0}$	$1.61^{+0.03}_{-0.00}$	(13),(2)
HD 81688[c]	$2.07^{+0.14}_{-0.16}$	$1.1^{+0.3}_{-0.2}$	$1.77^{+0.3}_{-0.2}$	$0.66^{+0.05}_{-0.05}$	(5),(2)
ϵ Tau[c]	$2.84^{+0.07}_{-0.16}$	$2.7^{+0.3}_{-0.2}$	$7.34^{+0.5}_{-0.4}$	$1.90^{+0.07}_{-0.05}$	(14),(2)
ξ Aql[c]	$2.29^{+0.27}_{-0.13}$	$1.4^{+0.2}_{-0.2}$	$2.02^{+0.2}_{-0.2}$	$0.58^{+0.02}_{-0.03}$	(5),(2)
NGC 2423[f]	$2.4^{+0.2}_{-0.2}$	$2.45^{+0.35}_{-0.25}$	$10.7^{+1.0}_{-0.7}$	$2.11^{+0.10}_{-0.07}$	(15)
NGC 4349[f]	$3.9^{+0.3}_{-0.3}$	$3.9^{+0.5}_{-0.5}$	$19.8^{+1.7}_{-1.7}$	$2.38^{+0.10}_{-0.11}$	(15)

Notes. $M_\star$, $M_p \sin i$, and a are the stellar mass, the planetary minimum mass, and the semimajor axis, respectively. NA means that under the assumption that the star is on its HeB or post-HeB, no theoretical track matches its luminosity and effective temperature in the H-R diagram. The samples listed above are stars with published values of masses $M_\star \geqslant 1.6\,M_\odot$ and radii $R_\star \simeq 10$–$20\,R_\odot$. When re-evaluating, we have assumed that the solar effective temperature is 5777 K and the solar metallicity is 0.02.
[a] Stellar masses, $M_\star$, in the literature.
[b] (1) Liu et al. (2008); (2) Takeda et al. (2008); (3) Döllinger et al. (2009); (4) Sato et al. (2008b); (5) Sato et al. (2008a); (6) Niedzielski et al. (2009); (7) de Medeiros et al. (2009); (8) Omiya et al. (2009); (9) Setiawan et al. (2005); (10) Sato et al. (2010); (11) Niedzielski et al. (2007); (12) Liu et al. (2009); (13) Hatzes et al. (2006); (14) Sato et al. (2007); (15) Lovis & Mayor (2007).
[c] Values of the effective temperature, $T_{\rm eff}$, and the luminosity, $L_\star$, and their errors have been taken from the references.
[d] Values and their errors of $L_\star$ have been derived form those of $T_{\rm eff}$ and the stellar radius, $R_\star$.
[e] Errors of $L_\star$ have been derived from those of $T_{\rm eff}$ and $R_\star$.
[f] Stellar masses have been determined so that the stellar ages match the observed cluster age, the stars being assumed to be in the HeB phase.

hydrodynamic simulations by Penev et al. (2007) demonstrate that the dependence is close to linear (i.e., $f \propto P/T$), which happens to be consistent with that proposed by Zahn (1966) who assumed that the largest eddy dominates tidal dissipation.

Figure 5 shows $a_{\rm crit}$ calculated for three different values of the power index $n = 0, 1,$ and 2 (solid lines) for $f = \min[1, (P/T)^n]$. It also plots the measured semimajor axes of the planets of interest. In calculating $a_{\rm crit}$, we assumed the planet's mass was $20\,M_J$, approximately the largest value of the minimum masses of planets presented in Figure 5. As n increases, the tidal dissipation becomes less efficient, when $P < T$. In other words, decreasing n moves the curve of $a_{\rm crit}$ upward in Figure 5. As seen in the figure, $a_{\rm crit}$ for $n = 1$ is larger by about 50% than that for $n = 2$ on the high-mass side. Note
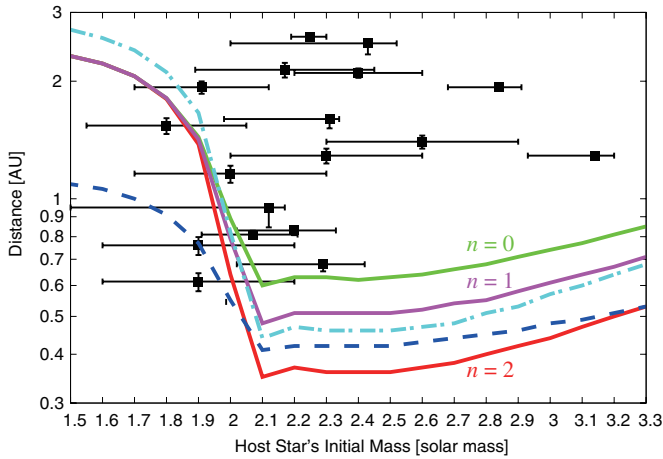
Figure 5. Impacts of uncertainties in turbulent viscosity and eccentricity on the critical initial semimajor axes. The three solid lines show the results with different frequency-dependent turbulent viscosities, namely, the power index, n, of $f = \min[1, (P/2T)^n]$ being 0, 1, and 2. The dashed line corresponds to the case with a constant quality factor $Q'_\star = 10^5$ (see the text for more details). The dash-dotted line corresponds to the case with a finite eccentricity of 0.25 (and $n = 2$). In these calculations, $Z_\star = 0.02$ and $M_p = 20\,M_J$. The symbols with error bars represent the semimajor axes of the planets detected around GK clump giants.

(A color version of this figure is available in the online journal.)

that $a_{\rm crit}$ hardly differs on the low-mass side, because $a_{\rm crit}$ is so large that P is almost always larger than T, namely, $f = 1$. In an extreme case of $n = 0$ (i.e., $f = 1$), $a_{\rm crit}$ is about twice as large as that for $n = 2$ on the high-mass side. Even in this case, decreasing n does not fill the gap.

Finally, we comment on the Q-prescription for stellar tide. Equation (1) can be written in the following form by using the quality factor, $Q'_\star$ (e.g., Goldreich & Soter 1966),

$$\frac{1}{a}\frac{da}{dt} = -\frac{9}{2}\left(\frac{G}{M_\star}\right)^{1/2}\frac{M_p}{Q'_\star}\frac{R_\star^5}{a^{13/2}} - \frac{\dot{M}_\star}{M_\star}. \qquad (8)$$

In this study, $Q'_\star$ varies with time, while $Q'_\star$ is often assumed to be constant ($=10^5\text{–}10^8$ for MS stars in the literature). Nordhaus et al. (2010) studied tidal engulfment mainly by AGB stars in cases of both variable $Q'_\star$ ($f = 1$) and constant $Q'_\star$ ($=10^5$). They found that the tidal decay rate in the former case is about four orders of magnitude higher than that in the latter case. In many cases in this study, $f = (P/2T)^2 \ll 1$, instead of $f = 1$. Thus, it would be worth checking the outcome for constant $Q'_\star$ in our high-mass cases. The dashed line in Figure 5 shows $a_{\rm crit}$ calculated by Equation (8) with $Q'_\star = 1 \times 10^5$. As seen in the figure, the tidal decay with $Q'_\star = 1 \times 10^5$ yields similar values of $a_{\rm crit}$ which we derive with variable $Q'_\star$ on the high-mass side. This means that the stellar tide with high $Q'_\star$ does not fill the gap either.

5.2. Stellar Evolution

There are several different stellar-evolution models in the literature, as mentioned in Section 2. We discuss the differences in terms of the survival limit and clarify the cause of the relatively big difference in $a_{\rm crit}$ between this study and Villaver & Livio (2009).

In Figure 6, the solid and dashed lines (without symbols) represent results that we have obtained using MESA with and without overshooting, respectively. The line with open circles is the result that we have calculated using Suda et al.'s (2007) code.
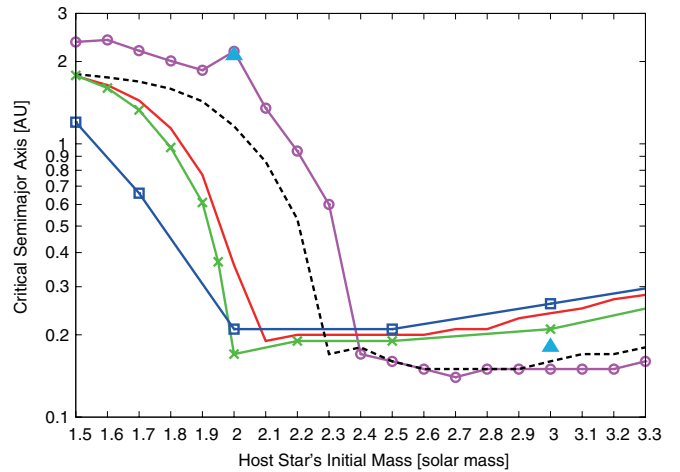
Figure 6. Critical initial semimajor axes as a function of stellar mass calculated with four different stellar-evolution codes. The solid and dashed lines are from MESA version 2258 (Paxton et al. 2011) with and without overshooting, respectively; the lines with crosses, open squares, and open circles are from Girardi et al.'s (2000), Lejeune & Schaerer's (2001), and Suda et al.'s (2007) codes, respectively; the filled triangles are from Villaver & Livio (2009). The critical initial semimajor axes (except for the triangles) have been calculated until the host star's RGB-tip under the assumption that $M_{\rm env} = M_\star$ and $R_{\rm env} = 0$ in the calculations of stellar tide (see Equations (2) and (4)) and that $\dot{M}_\star = 0$ in Equation (1). As for calculations with Girardi et al.'s (2000) code, we have assumed that $M_\star$ is constant with time because values of $M_\star$ as a function of time are unavailable.

(A color version of this figure is available in the online journal.)

The two triangles correspond to the values of $a_{\rm crit}$ from Villaver & Livio (2009). These two codes do not include overshooting. The lines with crosses and squares are the results calculated with grid data from Girardi et al. (2000) and Lejeune & Schaerer (2001), respectively, which include overshooting; these codes have been used to estimate the mass of planet-host clump giants.

When deriving $a_{\rm crit}$ in Figure 6, except for those from Villaver & Livio (2009), we have assumed that $M_{\rm env} = M_\star$ and $R_{\rm env} = 0$ when calculating quantities relevant to stellar tide, k and T (see Equations (2) and (4)), because no detailed information about the stellar internal structure is available. Such simplification certainly results in inaccurate evaluation of tidal dissipation (i.e., k/T), but the tidal dissipation factor was found to play a minor role in $a_{\rm crit}$ in Section 3.2; the most important factor is the stellar radius. This means that such simplification as to stellar structure does not affect our conclusions in this section.

We have figured out that the inclusion of overshooting probably causes the difference in $a_{\rm crit}$ between our calculations (solid line without symbol) and Villaver & Livio's (2009, triangles). Qualitatively, overshooting plays a role in mixing hydrogen and helium, so that stellar models with overshooting contain bigger helium cores compared to those without overshooting. This results in higher central temperatures, which prevent the helium core from being degenerated. This means that overshooting is effective in moving the sharp transition from the high-$a_{\rm crit}$ to the low-$a_{\rm crit}$ domain leftward in Figure 6. That is why we have obtained a value of $a_{\rm crit}$ quite different from that of Villaver & Livio (2009) for $M_\star = 2\,M_\odot$.

In any case, the drastic decrease in $a_{\rm crit}$ due to avoidance of the helium flash does occur, independent of the simulation code, although the threshold mass somewhat depends on the code. The difference in code never changes our conclusion concerning the survival limit.

5.3. Eccentricity

Since we are interested in semimajor axes of planets, we have integrated the equation for change in the semimajor axis (Equation (1)), ignoring eccentricity, following previous studies (e.g., Villaver & Livio 2009; Nordhaus et al. 2010). However, the planets detected around clump giants have finite eccentricities. Here we make a simple check of the impact of the finite eccentricity on the critical semimajor axis.

The dash-dotted line in Figure 5 shows $a_{\rm crit}$ for $e = 0.25$ which we have calculated by integrating the equation (e.g., see Hut 1981)

$$\frac{1}{a}\frac{da}{dt} = -6\frac{k}{T}\frac{M_p}{M_\star}\left(1 + \frac{M_p}{M_\star}\right)\left(\frac{R_\star}{a}\right)^8\frac{f_1(e^2)}{(1-e^2)^{15/2}} - \frac{\dot{M}_\star}{M_\star},$$

(9)

where

$$f_1(e^2) = 1 + \frac{31}{2}e^2 + \frac{255}{8}e^4 + \frac{185}{16}e^6 + \frac{25}{64}e^8.$$

(10)

The likelihood values of the eccentricities of inner planets ($a < 1.9$ AU) are smaller than 0.25. In this figure, it is demonstrated that incorporating the finite value of $e = 0.25$ does not affect our conclusion about the presence of the gap. Note that the evolution of e itself coupled with that of host stars' rotation is an interesting problem, which will be addressed in our future work.

6. STELLAR-MASS-DEPENDENT PLANET FORMATION

A possibility other than planet engulfment is that some stellar-mass-dependent processes hinder the formation of SPGPs around 1.5–3 $M_\odot$ stars. For example, ultraviolet measurements of young stars indicate that the stellar accretion rate ($\dot{M}_\star$) increases rather rapidly with stellar mass, namely, $\dot{M}_\star \propto M_\star^2$ (Calvet et al. 2004; Muzerolle et al. 2005). This implies that the lifetimes of protoplanetary disks of heavier stars are shorter. Based on this fact, Burkert & Ida (2007) supposed that protoplanetary disks could dissipate before giant planets migrate to the vicinity of the central stars in the case of F stars (1.2–1.5$M_\odot$). Then, they demonstrated that the idea worked to account for the observed period valley between the hot-Jupiter and cool-Jupiter classes. Applying the idea to heavier stars, Currie (2009) proposed that SPGPs are rarely formed around ∼1.5–3.0 $M_\odot$ stars.

However, the primordial origin of the paucity of SPGPs remains a matter of debate. The negative dependence of disk lifetime on stellar mass has not yet been confirmed theoretically. It is also controversial whether planetary migration occurs in disks for which such significant stellar accretion is observed. Furthermore, there are several competing factors that affect the frequency of the occurrence of SPGPs around ∼1.5–3 $M_\odot$ stars. More distant snowlines due to the high luminosity of such stars also tend to reduce the frequency (Ida & Lin 2005). By contrast, more massive disks and shorter Kepler periods at given semimajor axes form giant planets faster, which results in a higher production rate of SPGPs and suggests that the detection frequency of giant planets may be higher around high-mass stars (Omiya et al. 2009). Further detailed observational data on SPGPs will constrain the stellar mass dependence of planet formation.

7. SUMMARY AND CONCLUSIONS

In this study, we have derived the survival limit beyond which planets are engulfed by their host stars in the RGB and HeB phases by numerically simulating both the tidal evolution of planetary orbits and the evolution of the host stars. We have made a detailed comparison of the survival limit with the observed semimajor axes of planets detected around GK clump giants. This comparison demonstrates that (1) almost all the planets are orbiting exterior to our theoretical survival limit and (2) the planets around stars with relatively large masses of $\gtrsim 2.5\,M_\odot$ are far outside the survival limit. These facts suggest that planet engulfment by host stars may actually have happened, but it may never be the main reason for the observed lack of short-period planets around clump giants. Because the number of planets is statistically insufficient in this high-mass range, we have to say that our findings are not definite. The problem we addressed has a great influence on our understanding of planet formation. Therefore, further surveys for planets around clump giants are highly encouraged.

REFERENCES

Burkert, A., & Ida, S. 2007, ApJ, 660, 845
Calvet, N., Muzerolle, J., Briceño, C., Hernández, J., Hartmann, L., Saucedo, J. L., & Gordon, K. D. 2004, AJ, 128, 1294
Currie, T. 2009, ApJ, 694, L171
de Medeiros, J. R., et al. 2009, A&A, 504, 617
Döllinger, M. P., Hatzes, A. P., Pasquini, L., Guenther, E. W., & Hartmann, M. 2009, A&A, 505, 1311
Duncan, M. J., & Lissauer, J. J. 1998, Icarus, 134, 303
Girardi, L., Bressan, A., Bertelli, G., & Chiosi, C. 2000, A&AS, 141, 371
Goldreich, P., & Nicholson, P. D. 1977, Icarus, 30, 301
Goldreich, P., & Soter, S. 1966, Icarus, 5, 375
Goldstein, J. 1987, A&A, 178, 283
Hatzes, A. P., et al. 2006, A&A, 457, 335
Hut, P. 1981, A&A, 99, 126
Ida, S., & Lin, D. N. C. 2004a, ApJ, 604, 388
Ida, S., & Lin, D. N. C. 2004b, ApJ, 616, 567
Ida, S., & Lin, D. N. C. 2005, ApJ, 626, 1045
Ida, S., & Lin, D. N. C. 2008a, ApJ, 673, 487
Ida, S., & Lin, D. N. C. 2008b, ApJ, 685, 584
Ida, S., & Lin, D. N. C. 2010, ApJ, 719, 810
Kennedy, G. M., & Kenyon, S. J. 2008a, ApJ, 673, 502
Kennedy, G. M., & Kenyon, S. J. 2008b, ApJ, 682, 1264
Kippenhahn, R., & Weigert, A. 1990, Stellar Structure and Evolution (Berlin: Springer), 468
Lejeune, T., & Schaerer, D. 2001, A&A, 366, 538
Liu, Y.-J., Sato, B., Zhao, G., & Ando, H. 2009, Res. Astron. Astrophys., 9, L1
Liu, Y.-J., et al. 2008, ApJ, 672, 553
Livio, M. 1982, A&A, 112, 190
Livio, M., & Soker, N. 1983, A&A, 125, L12
Livio, M., & Soker, N. 1984, MNRAS, 208, 763
Lovis, C., & Mayor, M. 2007, A&A, 472, 657
Mordasini, C., Alibert, Y., & Benz, W. 2009a, A&A, 501, 1139
Mordasini, C., Alibert, Y., Benz, W., & Naef, D. 2009b, A&A, 501, 1161
Muzerolle, J., Luhman, K. L., Briceño, C., Hartmann, L., & Calvet, N. 2005, ApJ, 625, 906

Niedzielski, A., Gozdziewski, K., Wolszczan, A., Konacki, M., Nowak, G., & Zielinski, P. 2009, ApJ, 693, 276

Niedzielski, A., et al. 2007, ApJ, 669, 1354

Nordhaus, J., Spiegel, D. S., Ibgui, L., Goodman, J., & Burrows, A. 2010, MNRAS, 408, 631

Omiya, M., et al. 2009, PASJ, 61, 825

Paxton, B., Bildsten, L., Dotter, A., Herwig, F., Lesaffre, P., & Timmes, F. 2011, ApJS, 192, 3

Penev, K., Sasselov, D., Robinson, F., & Demarque, P. 2007, ApJ, 655, 1166

Rasio, F. A., Tout, C. A., Lubow, S. H., & Livio, M. 1996, ApJ, 470, 1187

Reimers, D. 1975, in Problems in Stellar Atmospheres and Envelopes, ed. B. Bascheck, W. H. Kegel, & G. Traving (New York: Springer), 229

Sackmann, I.-J., Boothroyd, A. I., & Kraemer, K. E. 1993, ApJ, 418, 457

Sato, B., Kambe, E., Takeda, Y., Izumiura, H., Masuda, S., & Ando, H. 2005, PASJ, 57, 97

Sato, B., et al. 2007, ApJ, 661, 527

Sato, B., et al. 2008a, PASJ, 60, 539

Sato, B., et al. 2008b, PASJ, 60, 1317

Sato, B., et al. 2010, PASJ, 62, 1063

Setiawan, J., et al. 2005, A&A, 437, L31

Suda, T., Fujimoto, M. Y., & Itoh, N. 2007, ApJ, 667, 1206

Takeda, Y., Sato, B., & Murata, D. 2008, PASJ, 60, 781

Vila, S. C. 1984, Earth Moon Planets, 31, 313

Villaver, E., & Livio, M. 2009, ApJ, 705, L81

Zahn, J. P. 1966, Ann. Astrophys., 29, 489

Zahn, J.-P. 2008, EAS Publ. Ser., 29, 67